Drug Delivery and Translational Research (2022) 12:3017–3028
https://doi.org/10.1007/s13346-022-01167-w

ORIGINAL ARTICLE

Baicalin-berberine complex nanocrystals orally promote the co-absorption of two components

Ziwei Li[1,2] · Yiting Liu[1,2] · Jilin Wang[1,2] · Xiaojiao Feng[1,2] · Ebuka-Olisaemeka Nwafor[1,2] · Ying Zhang[1,2] · Rui Liu[1,2] · Wenli Dang[1,2] · Qingqing Zhang[1,2] · Changxiang Yu[1,2] · Jiaxin Pi[1,2] · Zhidong Liu[1,2]

Accepted: 10 April 2022 / Published online: 27 April 2022

Abstract

Baicalin (BA)-berberine (BBR) have been proposed as the couple in the prevention and treatment of numerous diseases due to their multiple functional attributes. However, with regard to certain factors involving unsatisfactory aqueous solubility and low bioavailability associated with its clinical application, there is need for continuous researches by scientist. In this study, after successfully preparing BA-BBR complex, BA-BBR complex nanocrystals were obtained through high-pressure homogenization and evaluated (in vitro and in vivo). The particle size, distribution, morphology, and crystalline properties for the optimal BA-BBR complex nanocrystals were characterized by the use of scanning electron microscope, dynamic light scattering, powder X-ray diffraction, and differential scanning calorimetry. The particle size and poly-dispersity index of BA-BBR complex nanocrystals were 318.40 ± 3.32 nm and 0.26 ± 0.03, respectively. In addition, evaluation of the in vitro dissolution extent indicated that BA and BBR in BA-BBR complex nanocrystals were 3.30- and 2.35-fold than BA-BBR complex. Subsequently, single-pass intestinal perfusion combined with microdialysis test and oral pharmacokinetics in SD rats was employed to evaluate the in vivo absorption improvement of BA-BBR complex nanocrystals. The pharmacokinetics results exhibited that the area under curve of BA and BBR in the BA-BBR complex nanocrystals group were 622.65 ± 456.95 h·ng/ml and 167.28 ± 78.87 h·ng/ml, respectively, which were separately 7.49- and 2.64-fold than the complex coarse suspension. In conclusion, the above results indicate that the developed and optimized BA-BBR complex nanocrystals could improve the dissolution rate and extent and oral bioavailability, as well as facilitate the co-absorption of the drug prescriptions BA and BBR.

Keywords Baicalin-berberine complex · In vitro dissolution · Microdialysis · Nanocrystals · Single-pass intestinal perfusion

Introduction

Baicalin (BA) and berberine (BBR) are the main active components obtained from *Scutellaria baicalensis* and *Coptis chinensis*, respectively [1, 2]. The prescription compatibility of *Scutellaria baicalensis* and *Coptis chinensis* has been widely applied clinically in TCM for various purposes involving clearing away heat, dampness, purge fire, and detoxification. Also, modern pharmacological researches have demonstrated that the compatibility possesses several pharmacological actions such as antibacterial, antidiabetic, anti-tumor, hypoglycemic, and antioxidant [3–6].

Studies have found that the water extracts of CR and SR are clear and transparent, but mixing them will produce significant and massive precipitation [7], and the same phenomenon is widespread in the compatibility process of many drug pairs, such as Huanglian Jiedu Decoction [8], Xiexin Decoction [9], and Gegen Qinlian Decoction [10]. These famous formulas typically contained glycosides (baicalin) and alkaloids (berberine), traditional Chinese medicine components, exhibiting significant self-precipitation phenomenon during decoction [11] such as BA-BBR complex.

Yiting Liu and Ziwei Li contributed equally to this work.

✉ Jiaxin Pi
pijiaxin@tjutcm.edu.cn

✉ Zhidong Liu
liuzhidong@tjutcm.edu.cn

[1] State Key Laboratory of Component-Based Chinese Medicine, Tianjin University of Traditional Chinese Medicine, No. 10 Tuanbo New Town West District, Poyang Lake Road, Jinghai District, 301617 Tianjin, China

[2] Engineering Research Center of Modern Chinese Medicine Discovery and Preparation Technique, Ministry of Education, Tianjin 301617, China

Nowadays, although a few studies have proposed BA-BBR complex as an efficient mode of oral administration for the two components [12], the effectiveness still remains unsatisfactory due to the low bioavailability [13, 14]. Therefore, it is important to carry out continuous in-depth study, accordingly, to increase the potency of the aforementioned prescription clinically during oral administration.

The use of nanocrystal technology in pharmaceutical formulations has been significant particularly towards improving the dissolution rate and extent [15, 16], as well as the bioavailability of poorly soluble drugs [17–19]. However, at the moment, there are little or no studies regarding enhancing the oral co-absorption of the TCM prescription such as BA and BBR couple. Thus, the efficiency the nano-crystalized complex form towards improving the oral co-absorption of the two components should be deeply discussed.

In the course of this study, the BA-BBR complex was designed by using the technical means of nanocrystals. Furthermore, the oral absorption characteristics of BA and BBR co-delivery were carried out to investigate the positive effect of complex nanocrystal technology on improving the oral absorption of the two components.

Materials and methods

Chemicals and reagents

Baicalin (BA, 95.4% purity, 110,715–201,821) and berberine (BBR, 86.7% purity, 1,107,132–201,814) as standard were purchased from the National Institute for the Control of Pharmaceutical and Biological Products (Beijing, China) and Shanghai Yuanye Biological Technology Co. Ltd. (Shanghai, China), respectively. BA (purity ≥ 98%) and BBR (purity ≥ 98%) as drug substance were purchased from Nanjing Zelang Medical Technology Co. Ltd. (Nanjing, China). Methanol and other chromatographic reagents were obtained from Fisher Scientific Co. (New Jersey, USA). Other reagents utilized were of analytical grade.

Animals

Rats (Sprague–Dawley), weighing ~ 250 g, were obtained from SPF Biotechnology Co. Ltd, Beijing. They were maintained under controlled conditions, as well as allowed free access to water and pelleted diet. The processes involved in these biological experiments were approved by the Animal Research Ethics Committee of Tianjin University of Traditional Chinese Medicine (License No. TCM-LAEC2020075).

Preparation of BA-BBR complex nanocrystals

BA-BBR complex was obtained in accordance with prescription screening and previous publication [20]. Briefly, the BA and BBR molar ratios of 1:1 were added into the round bottom flask, and the appropriate amount of deionized water was added. After 1-h reaction at a suitable temperature, BA-BBR crude complex was obtained. BA-BBR complex with high purity was harvested after recrystallization with methanol.

Subsequently, BA-BBR complex nanocrystals were prepared by high-pressure homogenization (HPH) using the BA-BBR complex harvested above. The formula was selected by a single-factor test with particle size as evaluation index. The type and concentration of surfactants were screened to stabilize the drug substance. Firstly, Poloxamer188 (P188), Poloxamer407 (P407), d-α-tocopheryl polyethylene glycol 1000 succinate (TPGS), Tween-80, polyvinylpyrrolidone K30 (PVP-K30), and carboxymethyl cellulose (CMC) were respectively tried with a fixed dosage of 0.2% (w/v). Then, the formulation of P188 was further optimized at different concentrations (0.05, 0.1, 0.2, 0.3, 0.5% (w/v)). The stable BA-BBR complex nano-suspension was obtained by evaluating the pressure and cycles of homogenization. In order to improve the physical stability of nanometer water suspension, nano-suspension was freeze-dried with 3% (w/v) mannitol as the lyophilized protective agent. The suspension was pre-frozen in a refrigerator at − 80 °C for 24 h and then freeze-dried in FDU-2100 (Tokyo physicochemical Co. Ltd., Japan) for 24 h.

Particle size analysis

The hydrodynamic diameter of the BA-BBR complex nanocrystals was explored through dynamic light scattering (DLS) measurements using a light scattering apparatus (Nano ZS, Malvern Instruments, UK). An average of three measurements was considered as the data.

Differential scanning calorimetry (DSC)

In DSC studies, the thermal properties of BA and BBR, physical mixture of BA and BBR, BA-BBR complex, and complex nanocrystals formulation (prior to lyophilization) were analyzed using Jade-differential scanning calorimetry (Perkin Elmer, USA.) system. Samples (about 5 mg), were sealed in an aluminum pan and heated at a rate of 10 °C/min (30 ~ 300 °C) under nitrogen purge. The change of heat in samples was monitored with respect to temperature.

Powder X-ray diffraction (PXRD)

PXRD data of BA and BBR, physical mixture of BA and BBR, BA-BBR complex, and BA-BBR complex nanocrystals were recorded using a powder X-ray diffractometer (D/MAX-2550 V, Rigaku Co., Japan), with Cu-Kα radiation (Cu-Kα1 = 1.542 Å). The voltage and current of the tube

applied were 40 kV and 100 mA, respectively. Samples were placed on the sample holder, which has 1-mm thickness and 1.5 cm in diameter. With a scan rate of 5° per min, sample scan was performed continuously in locked coupled mode, ranging from 5 to 60°. MDI Jade 6.0 was utilized in plotting PXRD patterns.

Scanning electron microscope (SEM)

The morphology of BA, BBR, BA-BBR complex, and BA-BBR complex nanocrystals was conducted using scanning electron microscope (JSM-7500F, JEOL Ltd., Japan). The samples were covered with gold on a holder, desiccated in vacuum, and observed at different magnifications.

Evaluation of dissolution in vitro

The preparation method of dissolution medium

According to FDA guidance, the dissolution medium is formulated as follows:

Fasting simulated gastric fluid (FaSSGF): 0.58 g pepsin, 12.00 g sodium chloride, 0.056 g lecithin and 0.25 g sodium taurocholate in 6 L deionized water, adjusted pH value to 1.6 with 0.1 mol/L hydrochloric acid.
Fasting simulated intestinal fluid (FaSSIF): 8.38 g of sodium hydroxide, 0.55 g of lecithin, 24.00 g of sodium chloride, 13.36 g of maleic acid and 9.60 g of sodium taurocholate in 6 L deionized water, adjusted pH value to 7.3.

In vitro dissolution test

Dissolution of capsule containing BA-BBR complex or BA-BBR complex nanocrystals (BA 11.16 mg, BBR 10.02 mg) was performed in dissolution medium (900 ml), with dissolution testing apparatus (DT-820, ERWEKA Co., Germany) at 37 °C and speed of 100 rpm. FaSSGF and FaSSIF were employed as the dissolution medium. All dissolution analyses were carried out in triplicate. Two-milliliter aliquots of samples was withdrawn, alongside replacement at 5, 10, 15, 30, 45, 60, 90, 120, 180, and 240 min, respectively. Samples were filtered using 0.45-μm filter and analyzed. The concentration of drugs in each sample was determined by high-performance liquid chromatographic system (Shimadzu SIL-20AC, Japan), equipped with an Inertsil®ODS C_{18} (150×4.6 mm, 5 μm) column and a UV detector. Chromatographic separation was achieved with gradient elution using a mobile phase comprised of 0.2% formic acid in water (A) and acetonitrile (B). The HPLC gradient program was set as follows: 20–40% B at 0.0–5.0 min; 40–60% B at 5.0–10.0 min; 60–40% B at 10.0–15.0 min; and 40–20% B at 15.0–25.0 min. The column oven was maintained at 25 °C and the flow rate is 1 ml/min. The UV detector was set as 280 nm. A volume of 10 μl prepared samples was injected into the chromatographic system with the temperature of autosampler maintained at 4 °C. In addition, the limit of quantification of the two drugs was 0.1 μg/ ml.

Intestinal absorption studies in vivo

Preparation of single-pass intestinal perfusion samples and intestinal wall microdialysis samples

Prior to drug administration, the rats (Sprague–Dawley) were fasted for at least 12 h and allowed free access to water. Twelve rats were divided into two groups ($n=6$). Then, BA-BBR complex and BA-BBR complex nanocrystals were infused in each group, respectively.

The rats were anesthetized with urethane (Shanghai Macklin Biochemical Co., Ltd, Shanghai, China). The drug permeability in different regions of the specimen (particularly duodenum and jejunum) was measured by single-pass intestinal perfusion (SPIP) combined with microdialysis study. Following the opening of abdominal cavity, an intestinal loop (10 cm) was made at the two regions (duodenum and jejunum) by cannulation, and at same time, the microdialysis probe was implanted into the intestinal wall. The intestinal contents were removed by blank perfusion buffer. At the start of the study, perfusion solutions were perfused through the intestinal segment at flow rate of 0.2 ml/min for 30 min using a peristaltic pump (BT100-1L, Longer Precision Pump Co., Ltd.). Upon reaching a steady state, the intestinal perfusate samples were collected at 15-min intervals, for a duration of 2 h in glass vials. The glass vials were weighed before and after the perfusion. At same time, the microdialysis perfusion flow rate was set at 2.5 μl/min, and dialysis samples were collected at the exit every 20 min for 2 h.

The length of the perfused intestinal segments was accurately measured at the end of the experiment. The intestinal absorption parameters like effective permeability coefficient (P_{eff}) was calculated using the following Eqs. (1) [21]:

$$P_{eff} = \frac{-Q \cdot \ln(\frac{C_{out}V_{out}}{C_{in}V_{in}})}{2\pi rL} \quad (1)$$

In the above formula, P_{eff} represents the effective permeability coefficient (cm/min); Q_{in} flow rate of inlet solution, ml/min; C_{in} concentration of the drug in inlet solution, mg/ml; C_{out} concentration of the drug in exiting solution, mg/ml; V_{in} volume of the drug in inlet solution, ml; V_{out} volume of drug in the exiting solution, ml; L length of the intestinal segment, cm; and r radius of the intestinal segment, cm.

Sample determination and statistical analysis

All perfused solutions, including samples from both inlet and outlet drug solutions at different time points, were assayed using HPLC. The chromatographic conditions are the same as in vitro dissolution test. The intestinal wall of microdialysis samples were injected into LC–MS system for determination. The chromatographic separation was performed using a 6460 triple quadruple mass spectrometer (Agilent Technologies, USA). The 5 µL of sample was injected into the ESI source by ACQUITY UPLC® HSS T3 (50 mm × 2.1 mm, 1.8 µm, Waters, CA, USA). The mobile phase comprising of 0.1% formic acid in water (A) and acetonitrile (B) in a gradient proportion was prepared to separate the analytes from endogenous components. The time concentration (gradient setting) of the mobile-phase time was as follows: 25% → 32%, B (0.0–4.0 min); 32% → 50%, B (4.1–9.0 min); 50% → 25%, B (9.0–9.5 min); and 25%, B (9.5–11.0 min). The flow rate was 0.3 ml/min. Nitrogen served as the collision gas. All microdialysis samples of intestinal wall were tested in positive ionization mode at 4.0 kV (electrospray voltage) and 350 °C of capillary temperature. The quantitative parameters of the analysis are highlighted in Supplementary Data (Table S1).

SPSS software was used to carry out to analyze the variance of data. All data were expressed as means ± SD. $P \leq 0.05$ was determined to have significant difference. The difference between groups was compared by independent sample *t*-test.

In vivo pharmacokinetics

Preparation of plasma samples

Prior to administration, Sprague–Dawley rats (male, weighted ~ 250 g) were maintained under controlled conditions (fasted for at least 12 h and allowed free access to water).

For the pharmacokinetic study, twelve rats were randomly grouped into two ($n = 6$). Six rats in each group were orally administered BA-BBR complex or BA-BBR complex nanocrystals at a dose of 80 mg/kg, respectively. After oral administration, blood samples were collected from the venous plexus into tubes containing heparin sodium at different time points (0.08, 0.25, 0.5, 0.75, 1, 1.5, 2, 3, 4, 6, 8, 10, 12, and 24 h). Finally, the plasma was obtained by centrifugation at 4000 rpm for 10 min, and stored at − 80 °C until analysis.

Processing of the plasma samples

One hundred microliters of each plasma sample was spiked with carbamazepine (CBZ, as internal standard) methanol solution (200 µl, 1.0 µg/ml). Afterwards, the mixtures were vortexed (3 min), and centrifuged for 10 min at 12,000 rpm to extract the supernatant. Finally, 5 µl of the supernatant solution was injected into LC–MS/MS to determine the content of BA and BBR in plasma [22].

Determination of BA and BBR contents in plasma using UPLC-MS/MS

Chromatographic conditions

The chromatographic separation was performed using a 6460 triple quadruple mass spectrometer (Agilent Technologies, USA), equipped with electrospray ion source. The 5 µl of sample was injected into the ESI source by ACQUITY UPLC® HSS T3 (50 mm × 2.1 mm, 1.8 µm, Waters, CA, USA). The mobile phase comprising of solvent A (formic acid, 0.1%) and solvent B (acetonitrile) in a gradient proportion was prepared to separate the analytes from endogenous components. The time concentration (gradient setting) of the mobile phase time was as follows: 10% → 30%, B (0.0–7.0 min); 30% → 90%, B (7.0–9.0 min); 90% → 10%, B (9.0–10.0 min); and 10%, B (10.0–12.0 min). The flow rate was 0.3 ml/min, whereas the total run time was 12.0 min. Nitrogen served as the collision gas. BA, BBR, and the internal standard were analyzed using MRM scan mode. All samples were tested in positive ionization mode at 4.0 kV (electrospray voltage) and 350 °C of capillary temperature [23]. The quantitative parameters of the analysis are highlighted in Supplementary Data (Table S2).

Methodological validation

The analytical methods of plasma samples were validated accordingly (specificity, linearity, accuracy, precision, recovery, matrix effect, and stability).

To evaluate specificity, the BA, BBR, blank plasma, methanol, and IS were evaluated for any interference from unwanted plasma components at the elution time. The calibration curves were assessed using the standard range (10–5000 ng/ml) for BA and BBR (2–1000 ng/ml) to evaluate the linearity. Linear regression was carried out using 1/x as a weighting factor. On the same day, three consecutive data were analyzed respectively, to assess the intra-day and inter-day precision and accuracy by relative error and relative standard deviation. The extraction recoveries of BA and BBR were estimated, by comparing the peak area ratio of two analytes extracted from QC samples [BA (20, 500, 4000 ng/ml) and BBR (4, 100, 800 ng/ml)], against those obtained from the analytes dissolved in supernatant of the processed blank plasma. The matrix effects were evaluated by comparing the peak areas of extracted blank plasma against the standard solutions at equivalent concentrations.

Data analysis

The pharmacokinetic parameters of BA and BBR were determined using Phoenix Winnonlin6.4.

Results and discussion

Formulation of BA-BBR complex nanocrystals

In this study, the solution of BA-BBR complex prepared by precipitation method is in yellow suspension state [24], and yellow precipitation occurs after static state. After recrystallization with methanol, acicular or snowflake BA-BBR complexes were precipitated.

Nanocrystals are mainly composed of drugs and stabilizers, and their amorphous suspensions are colloidal dispersion systems. The preparation process of nanocrystals can be divided into bottom-up method and top-down method. Bottom-up method is a method to control the drug nanocrystallization process and drug precipitation formation process according to the morphology of drug molecules. The main methods include precipitation method, and the top-down law is to crush large particle size powder into nanoscale particles by mechanical force, including medium grinding method and HPH method [21, 25]. In this study, the HPH method was adopted, and 0.2% P188 was selected as the stabilizer to maintain the stability of the drug in the nanosystem. The preparation process is shown in Fig. 1.

Particle size analysis

Before freeze-drying, the particle size and polydispersity index of BA-BBR complex nanocrystals are 318.40 ± 3.32 nm and 0.26 ± 0.03, respectively. After freeze-drying, the particle size and polydispersion index of the BA-BBR complex nanocrystals are 416.40 ± 5.02 nm and 0.28 ± 0.04, respectively. The particle size distribution of BA-BBR complex nanocrystals is shown in Fig. 2.

Scanning electron microscope (SEM)

The surface morphology of BA, BBR, BA-BBR complex, and the BA-BBR complex nanocrystals are presented in Fig. 3. BA (Fig. 3A) is irregular crystals; BBR (Fig. 3B) is rectangular block crystal with rough cracks, whereas the BA-BBR complex (Fig. 3C) showed a remarkable change into long-rectangular rod structure. This phenomenon may be due to a series of intermolecular forces between BA and BBR in BA-BBR complexes (e.g., hydrophobic association and stacking of electrostatic attraction hydrogen bonds) [24]. The BA-BBR complex nanocrystals (Fig. 3D) show short round rod-like structures, which may be due to the formation of the BA-BBR complex under high pressure.

Differential scanning calorimetry (DSC)

To evaluate the possible change of crystal state during HPH, BA, BBR, BA-BBR physical mixture, BA-BBR complex, and BA-BBR complex nanocrystals were analyzed by DSC.

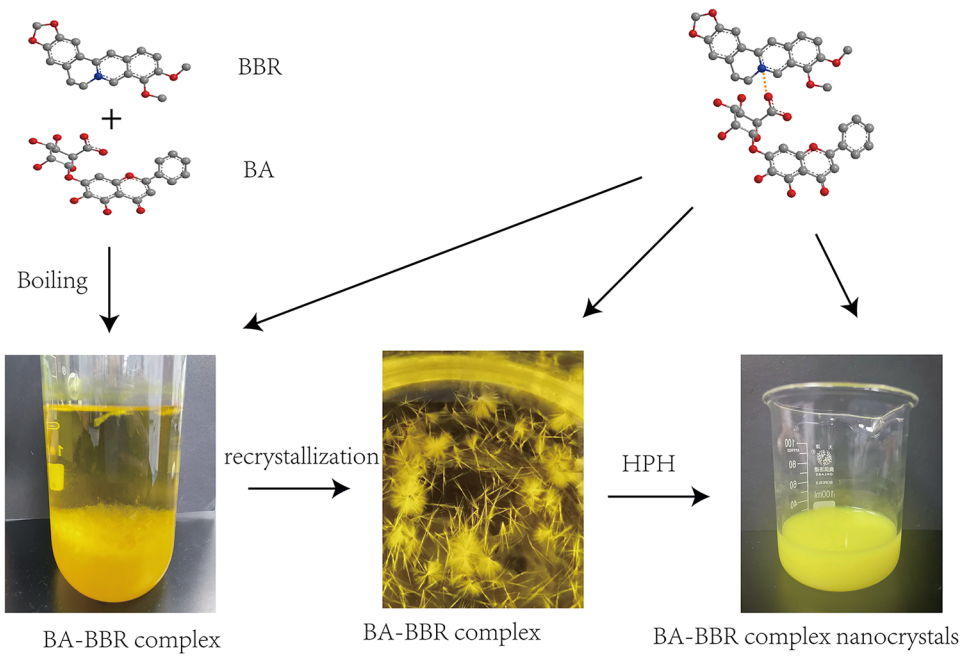

Fig. 1 Preparation process of BA-BBR complex nanocrystals

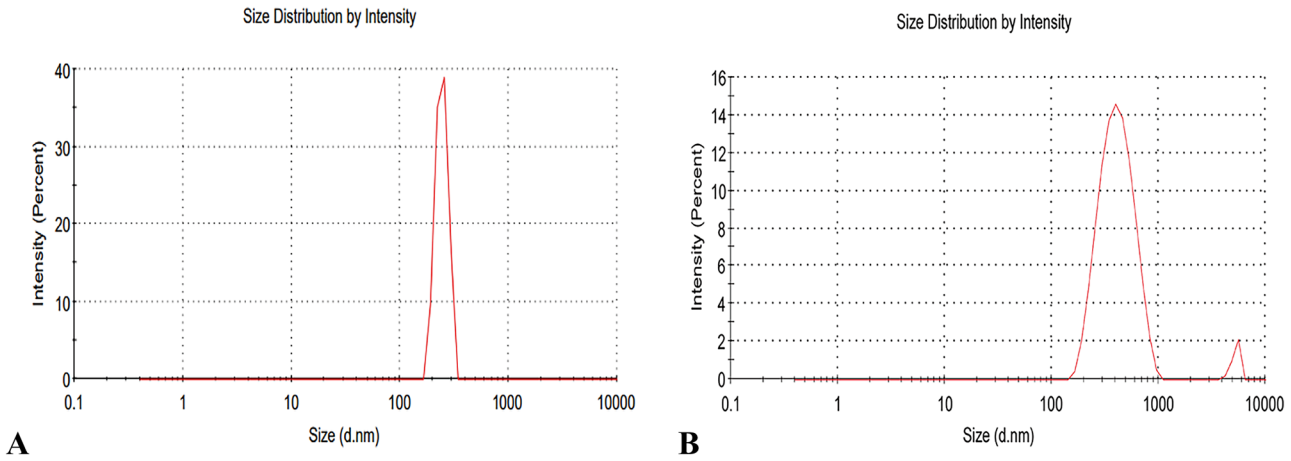

Fig. 2 Particle size distribution of BA-BBR complex nanocrystals before **A** and after **B** freeze-drying reconstitution

Heat maps of the different samples used for measurement are shown in Fig. 4. BA coarse has a sharp endothermic peak at 214.16 °C, which is consistent with the reported thermal behavior [26]. BBR coarse has a sharp endothermic peak at 198.03 °C, which is consistent with previous studies [27]. BA-BBR physical mixture has an endothermic peak at 184.20 °C, and the crystallinity of the physical mixture decreases. This peak is most likely the melting system formed during the heating process of the mixture. The BA-BBR complex has a new but weak endothermic peak. It is possible that some complex are irregularly arranged as they crystallize, resulting in reduced crystallinity. BA-BBR complex nanocrystals have no obvious characteristic peaks, which is due to their amorphous state.

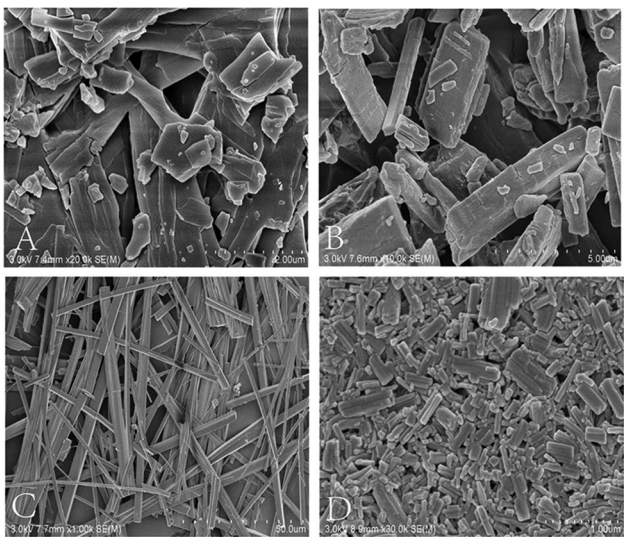

Fig. 3 Scanning electron microscopy of BA **A**, BBR **B**, BA-BBR complex **C**, BA-BBR complex nanocrystals **D**

Powder X-ray diffraction (PXRD)

BA-BBR was further identified by PXRD to ascertain whether the crystalline state of nanocrystals changes during HPH and freeze-drying. The PXRD patterns of BA, BBR, BA-BBR physical mixture, BA-BBR complex, and BA-BBR complex nanocrystals are shown in Fig. 5. As shown in the figure, the characteristic diffraction peaks of BA-BBR complex at 6.59°, 8.14°, 10.18°, 12.21°, 12.52°, 13.11°, 16.23°, and 18.08° indicate the crystallization state of BA-BBR complex, and its characteristic peaks are significantly different from those of the BA-BBR physical mixture. BA-BBR complex nanocrystals in 5.67°, 9.40°, 14.13°, 14.56°, 19.13°, 23.34°, 25.77°, and 26.30° characteristic peak, BA-BBR complex nanocrystals characteristic peak weakened or disappeared, explains the process of high-pressure homogeneous, BA-BBR complex nanocrystals state changes have taken place in, and parts of BA-BBR complex nanocrystals from crystallization state to amorphous state.

In vitro dissolution test

Figure 6 illustrates the dissolution extent of BA-BBR complex compared with BA-BBR complex nanocrystals in vitro under the conditions of fasting simulated gastric and intestinal fluid.

In FaSSGF, the results showed that the dissolution extent of BA was increased from 26.61 ± 10.71 to 87.88 ± 5.03%, as well as BBR improved from 39.71 ± 9.11 to 93.36 ± 2.50%. BA and BBR in the BA-BBR complex nanocrystals group were 3.30- and 2.35-fold than of the complex, respectively. The differences were extremely significant ($p < 0.01$).

In FaSSIF, the results exhibited that dissolution extent of BA and BBR in BA-BBR complex is 54.95 ± 19.00% and 40.28 ± 10.48%; the dissolution extent of BA and BBR

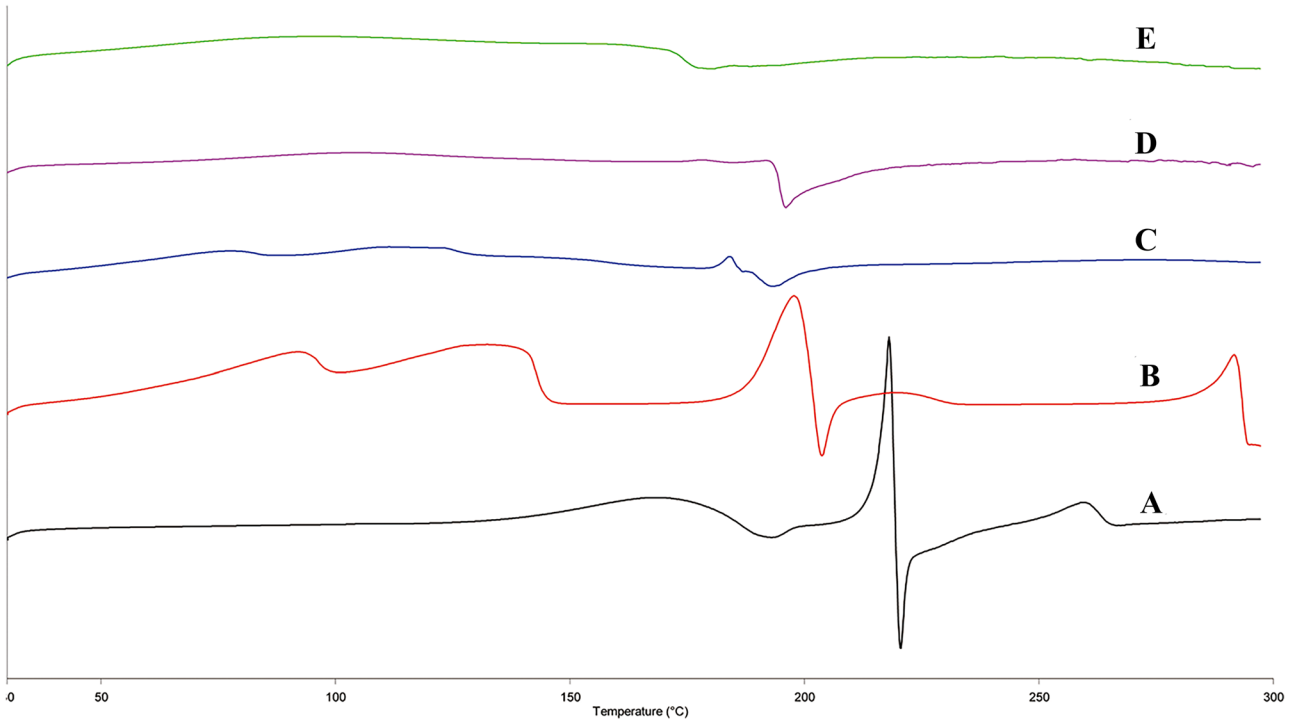

Fig. 4 DSC curves of BA **A**, BBR **B**, BA-BBR physical mixture **C**, BA-BBR complex **D**, BA-BBR complex nanocrystals **E**

in BA-BBR complex nanocrystals is 94.00 ± 10.03% and 65.22 ± 7.18%. BA and BBR in BA-BBR complex nanocrystals group were 1.71- and 1.62-fold than the complex, with extremely significant differences ($p < 0.01$).

The dissolution extent enhancement of BA-BBR complex nanocrystals from the above results showed mainly attribute to the reduced particle size. Due to widespread acceptance, particle size reduction, especially in the nanometer range, can produce a significant increase in the surface area. In accordance with Noyes-Whitney equation [28], the dissolution extent is proportional to the surface area. In addition, according to Prandtl equation [29], for very small particles, the diffusion distance decreases, which is another reason for the increase in dissolution. In addition, P188, as a stabilizer in the BA-BBR complex nanocrystal formulation, improves the wettability of the particles, thereby reducing the contact angle between the drug and the dissolved medium [30].

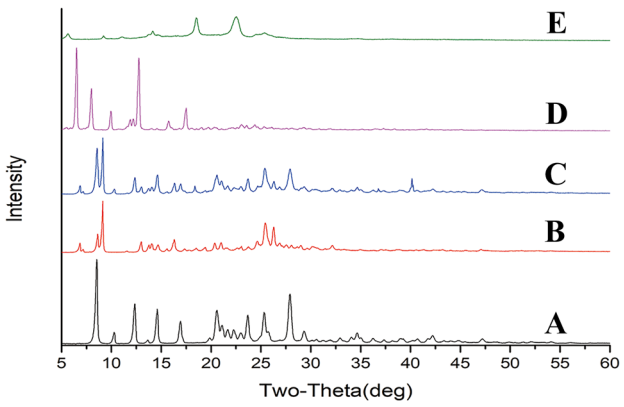

Fig. 5 X-ray diffraction of BA **A**, BBR **B**, BA-BBR physical mixture **C**, BA-BBR complex **D**, and BA-BBR complex nanocrystals **E**

Intestinal absorption studies in vivo

SPIP, which is used to measure the reduction in medication, is a classic technique for evaluating drug absorption [31]. However, there is still uncertainty about whether the drug is actually absorbed. Therefore, microdialysis needle implantation was carried out in the intestinal wall at the same time of SPIP to confirm the "real-time" entry of drugs reduced by SPIP into the intestinal wall [32]. In this study, microdialysis combined with SPIP technology was used to measure the transfusions and absorption amounts of two components of BA-BBR complex and BA-BBR complex nanocrystals through intestinal wall after unidirectional enteric perfusion and to evaluate the effects of BA-BBR complex nanocrystals on oral intestinal absorption. In the intestinal wall microdialysis experiment, the concentration of BA and BBR could be detected in the dialysis solution, and the results are shown in Table 1. The result of SPIP and intestinal wall microdialysis can be seen from Fig. 7, the concentration of the two active components of BA-BBR complex and BA-BBR complex

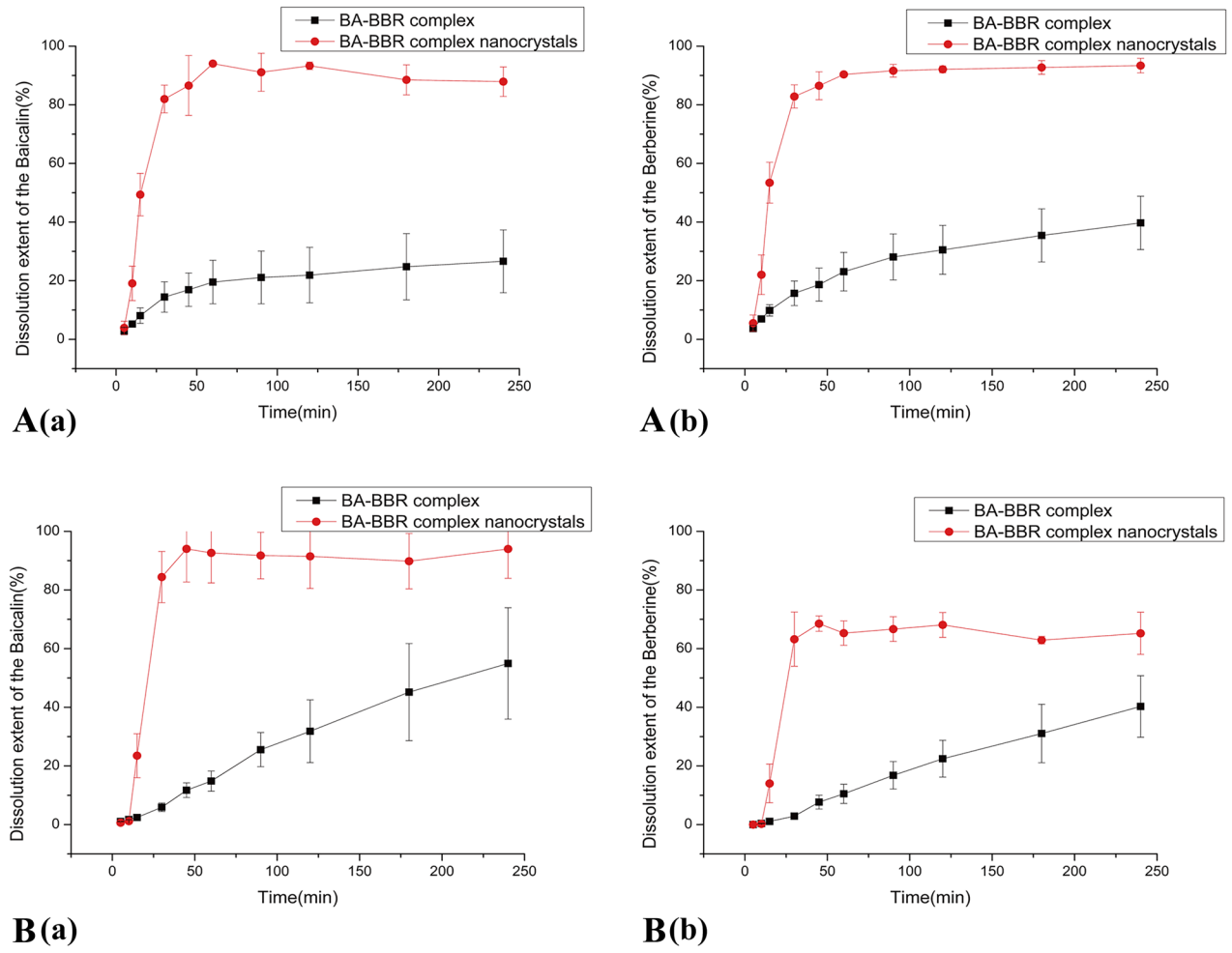

Fig. 6 Cumulative dissolution extent of BA **(a)** and BBR **(b)** in BA-BBR complex and BA-BBR complex nanocrystals in FaSSGF (**A**) and in FaSSIF (**B**) (mean ± SD, $n = 3$)

nanocrystals increased significantly after 20 min, and a relatively stable fluctuation occurred after 60 min. An average concentration of dialysis solution for 60 to 120 min was calculated, and in duodenum, BA and BBR in BA-BBR complex nanocrystals were 8.77- and 2.79-fold of BA-BBR complex, respectively. In jejunum, compared with BA-BBR complex, BA and BBR in BA-BBR complex nanocrystals increase by 4.08- and 2.20-fold, respectively. It can be seen that the BA-BBR complex nanocrystals significantly increased the amount of absorption than that of BA-BBR complex.

The absorption parameters, P_{eff} value of BA-BBR complex and BA-BBR complex nanocrystals in duodenum

Table 1 The concentration of each component in the microdialysis samples of duodenum and jejunum at different time points (mean ± SD, $n = 3$)

Time(min)	The concentration of dialysis samples in duodenum (ng/ml)				The concentration of dialysis samples in jejunum (ng/ml)			
	Complex nanocrystals		Complex		Complex nanocrystals		Complex	
	BA	BBR	BA	BBR	BA	BBR	BA	BBR
20	105.79 ± 114.8	499.16 ± 625.15	50.90 ± 84.71	79.03 ± 103.14	258.16 ± 340.61	967.21 ± 807.60	135.61 ± 128.80	495.29 ± 696.74
40	966.14 ± 292.23	2413.73 ± 428.12	139.85 ± 143.14	369.53 ± 617.36	338.46 ± 121.50	1044.32 ± 1314.14	88.80 ± 148.07	415.96 ± 500.47
60	888.37 ± 738.49	2188.80 ± 588.21	85.71 ± 99.11	559.85 ± 557.35	1444.75 ± 353.94	1737.02 ± 538.34	339.32 ± 444.80	361.67 ± 659.54
80	1090.40 ± 343.80	2205.57 ± 532.56	84.98 ± 95.28	930.27 ± 774.52	1166.35 ± 397.94	2043.02 ± 667.32	101.19 ± 135.85	667.18 ± 342.16
100	1199.96 ± 127.36	2230.18 ± 369.45	94.69 ± 122.47	826.80 ± 803.49	1215.53 ± 774.84	1890.40 ± 840.70	619.33 ± 799.00	1136.07 ± 685.02
120	948.52 ± 372.36	2137.12 ± 557.73	205.09 ± 315.59	822.20 ± 817.30	962.59 ± 107.06	1513.21 ± 411.67	114.12 ± 110.48	1106.47 ± 535.75

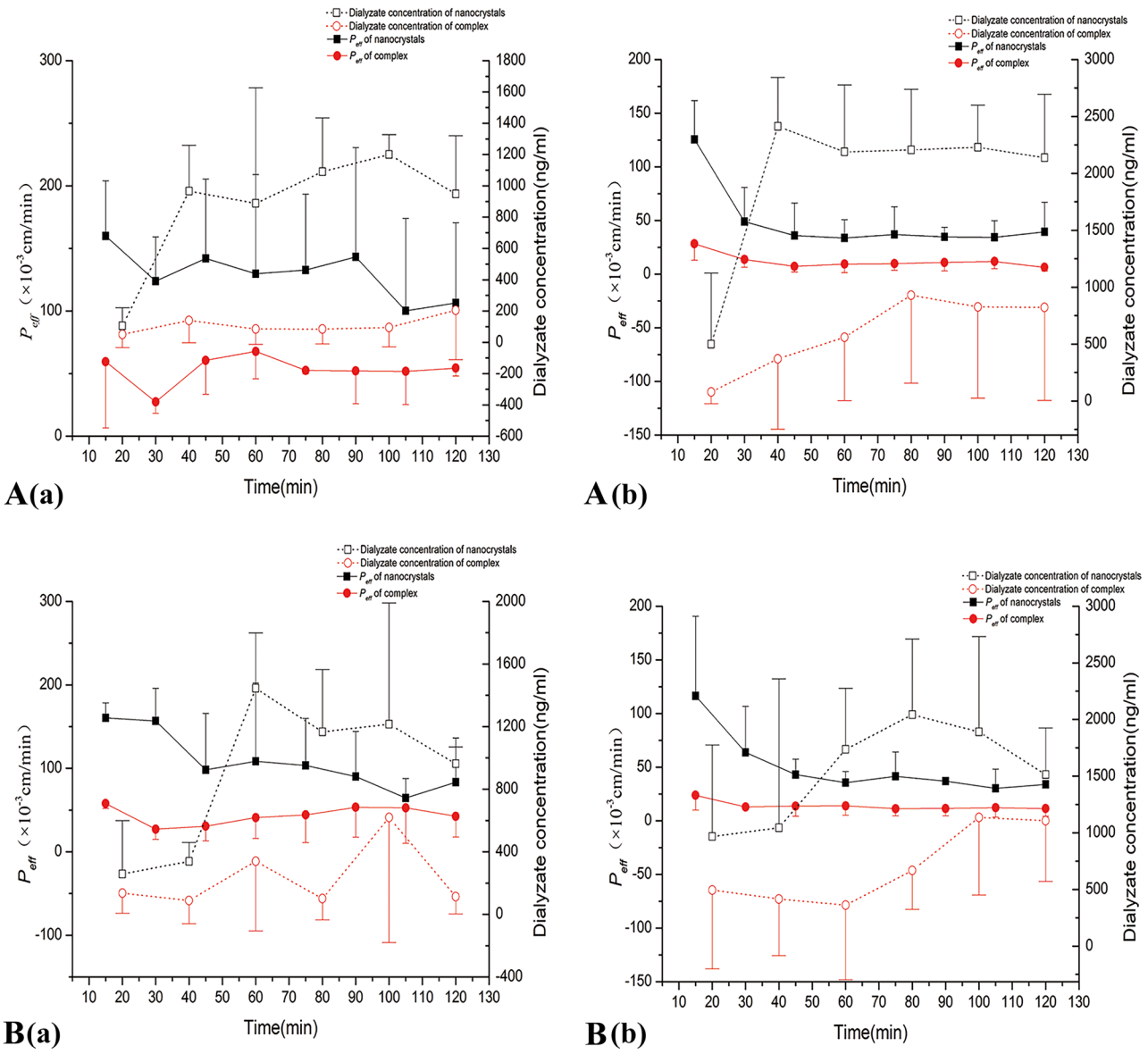

Fig. 7 Microdialysis and absorption of BA **(a)** and BBR **(b)** after perfusion of BA-BBR complex and BA-BBR complex nanocrystals in duodenum (**A**) and in jejunum (**B**) in rats (mean ± SD, $n = 3$)

and ileum are listed in Table 2. BA of BA-BBR complex nanocrystals of P_{eff} value was $(144.47 \pm 32.55) \times 10^{-3}$ cm·min^{-1} and $(109.64 \pm 35.50) \times 10^{-3}$ cm·min^{-1}, in duodenum and ileum, respectively. The P_{eff} value of BA in complex nanocrystals group was 2.55- and 2.63-fold of that in complex group, respectively, with significant differences ($p < 0.05$).

BBR of BA-BBR complex nanocrystals of the P_{eff} value was $(39.13 \pm 15.24) \times 10^{-3}$ cm·min^{-1} and $(40.70 \pm 14.97) \times 10^{-3}$ cm·min^{-1}, respectively. The P_{eff} value of BBR in complex nanocrystals group was 4.19- and 3.26-fold of that in complex group, respectively. There were significant differences ($p < 0.05$).

Results of the study combined with microdialysis showed that the amount and rate of absorption were significantly increased in BA-BBR complex nanocrystals than BA-BBR complex. Therefore, nanocrystalline technology can effectively promote the co-absorption of BA and BBR components.

Methodological validation

As shown in Fig. S1 of the "Supporting information," there were no obvious interference observed at the retention time of the analytes and IS due to endogenous substances in blank plasma. The contents of BA, BBR, and internal

Table 2 Steady-state effective permeability coefficient (P_{eff}) of components in BA-BBR complex and BA-BBR complex nanocrystals in duodenum and jejunum of rats ($\times 10^{-3}$ cm·min^{-1}, mean ± SD, $n = 3$)

Intestinal segment	BA		BBR	
	Complex	Complex nanocrystals	Complex	Complex nanocrystals
Duodenum	56.55 ± 3.63	144.47** ± 32.55	9.34 ± 6.11	39.13* ± 15.24
Jejunum	41.68 ± 22.92	109.64* ± 35.50	12.47 ± 6.98	40.70* ± 14.97

*$p < 0.05$, compared with BA-BBR complex group; **$p < 0.01$, compared with BA-BBR complex group

standard (CBZ) in blank plasma were not affected by the retention time of other components. The regression equation, linear range, and correlation coefficient are shown in Supporting information Table S3. All calibration curves demonstrated a significant linear relationship with correlation coefficient. Within the concentration range, intra-day and inter-day precision of the method were ≤ 2.87%, which indicated that the precision of the method met the requirement of content determination. When BA concentration was 20.36, 509.00, and 4072.00 ng/ml, respectively, the accuracy was less than 8.08%, and when BBR concentration was 3.96, 99.00, and 792.00 ng/ml, respectively, the accuracy was less than 5.31%, which met the analytical requirements of biological samples (shown in Supporting information Table S4). In Supporting information Table S5, the recoveries of BA and BBR were 70.81–92.95% and 88.57–104.34%, respectively, and the matrix effects were 74.69–91.81% and 68.14–78.54%, respectively, which met the experimental requirements of biological samples. Stability of BA and BBR in rat plasma under suitable conditions (listed in Supplementary Supporting information Table S6). The results proved that all analytes in rat plasma were stable during storage, at ambient temperature of 6 h for 30 days under 20 °C, freeze–thaw (3 times), and in autosampler at 4 °C for 24 h, respectively. This stability would satisfy the requirements of a routine pharmacokinetic studies.

Oral pharmacokinetic studies

The pharmacokinetics of BA-BBR complex nanocrystals and BA-BBR complex suspension in rats were studied. The drug concentration–time curves are shown in Fig. 8, whereas the relevant pharmacokinetic parameters are shown in Table 3.

The time of maximum concentrations (T_{max}) for BA-BBR complex nanocrystals is smaller compared with BA-BBR complex, which can reflect the rapid absorption of drugs and rapid effect in the body. The maximum plasma concentration (C_{max}) of BA and BBR in BA-BBR complex nanocrystals was significantly increased compared with that of BA-BBR complex suspension group, which was about 7.3- and 2.49-fold. The $AUC_{0\text{-}t}$ of BA and BBR in BA-BBR complex nanocrystals was 6048.52 ± 2203.83 h·ng/ml and 1271.40 ± 400.28 h·ng/ml, respectively, which was about 7.49- and 2.64-fold compared with that of BA-BBR complex suspension group. According to these results, BA-BBR complex nanocrystals have higher oral bioavailability than BA-BBR complex suspension and were consistent with the results of in vitro dissolution and SPIP combined with microdialysis test.

It can be seen from the drug concentration–time curves that the nanocrystals formed can significantly improve the absorption and dissolution rate and extent of BA and BBR. During the whole drug administration process, the $AUC_{0\text{-}t}$ of BA and BBR in the complex nanocrystals is always higher than that

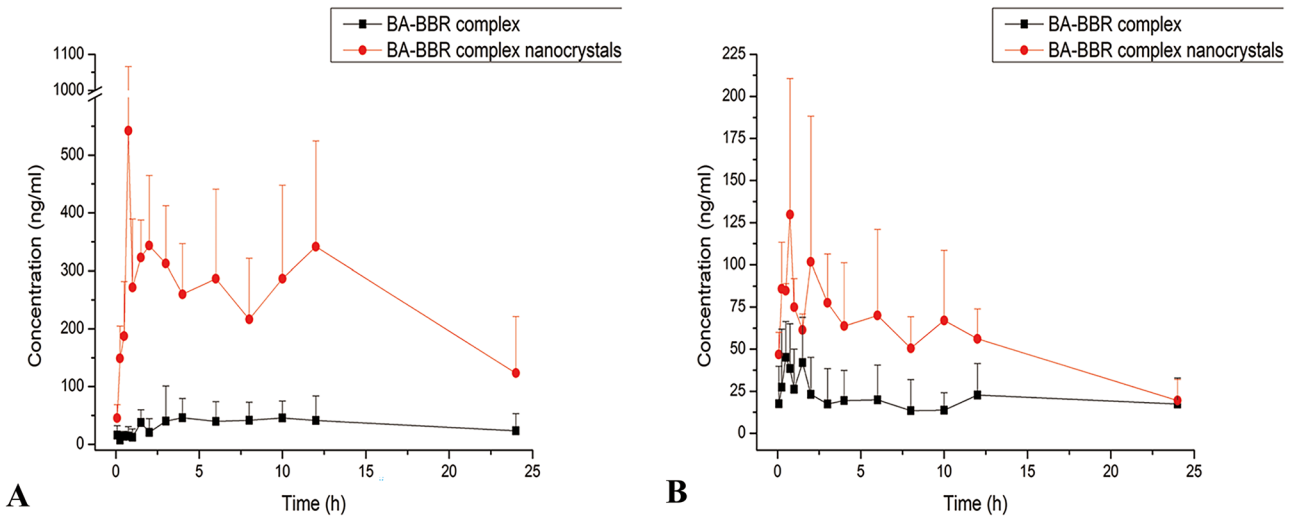

Fig. 8 AUC profiles of BA-BBR complex and BA-BBR complex nanocrystals after oral administration in rats (**A** BA, **B** BBR, mean ± SD, $n = 6$)

Table 3 Pharmacokinetic parameters of BA and BBR in rats after oral administration of BA-BBR complex and BA-BBR complex nanocrystals (mean ± SD, $n = 6$)

Analyte		BA		BBR	
Parameter	Unit	BA-BBR complex	BA-BBR complex nanocrystals	BA-BBR complex	BA-BBR complex nanocrystals
C_{max}	ng/ml	85.35 ± 46.37	622.65* ± 456.95	67.89 ± 13.41	167.28* ± 78.87
T_{max}	h	6.42 ± 5.20	3.17 ± 5.36	2.64 ± 4.63	0.79 ± 0.62
AUC_{0-t}	h·ng/ml	807.73 ± 558.75	6048.52** ± 2203.83	482.03 ± 196.17	1271.40** ± 400.28
L_z	1/h	0.27 ± 0.15	0.11 ± 0.12	0.06 ± 0.03	0.10 ± 0.07
$AUMC_{0-t}$	h·h·ng/ml	8967.29 ± 8312.57	61,506.29** ± 19,970.91	5412.1 ± 2319.3	11,406.24** ± 3257.06
$T_{1/2}$	h	3.00 ± 1.68	45.55 ± 76.10	15.78 ± 10.73	13.03 ± 10.78
Vz/F	l/kg	390.38 ± 412.06	116.32 ± 100.88	1450.37 ± 760.33	401.71* ± 246.30
CL/F	l/h/kg	75.42 ± 52.94	4.26* ± 2.00	70.80 ± 28.74	24.74** ± 8.78
MRT	h	9.46 ± 5.11	10.38 ± 1.66	11.25 ± 1.62	9.14 ± 1.71

*$p < 0.05$, compared with BA-BBR complex group; **$p < 0.01$, compared with BA-BBR complex group

of the complex, which shows the advantage of nanocrystals technology in promoting the insoluble components.

The increased bioavailability of BA-BBR complex nanocrystals can be attributed to increased solubility. In addition, reducing particle size to nanometer can increase the time for drug particles to adhere to the intestinal wall and increase the time for drug absorption in the intestinal tract. All the above reasons promote the co-absorption of BA and BBR.

Conclusion

In this study, novel hybrid complex nanocrystals of two components BA and BBR were successfully designed and fabricated by the use of HPH. Then, the characteristics (in vitro) and performance (in vivo) were investigated. The results of in vitro dissolution test showed a significant dissolution extent increase of two components in BA-BBR complex nanocrystals. The in vivo intestinal absorption and permeability of BA-BBR complex nanocrystals were significantly improved, and both components were simultaneously analyzed increase in the microdialysis samples from intestinal wall. Furthermore, pharmacokinetic studies have demonstrated a faster absorption rate and improved oral bioavailability of two compounds in BA-BBR complex nanocrystals compared with BA-BBR complex. In conclusion of this study, according to a couple of "medicine" in TCM, this study successful design of BA-BBR complex nanocrystals to manifest the dissolution extent increase, intestinal permeability, and bioavailability enhancement. Based on these findings, complex formation combined with nanocrystalline technology is an effective and promising strategy for improving oral bioavailability of multiple insoluble Chinese medicine components such as BA and BBR, providing a way of thinking and development of novel delivery for multiple components in Chinese medicine.

Supplementary information The online version contains supplementary material available at https://doi.org/10.1007/s13346-022-01167-w.

Author contribution JXP and ZDL conceived of the presented idea and designed the study. ZWL, YTL, JLW, and XJF performed the experiments. YTL and YZ contributed to the analysis of date. ZWL and EON wrote the manuscript. RL, WLD, QQZ, and CXY reviewed and edited the manuscript. All authors read and approved the final manuscript.

Funding This study was financially supported by the National Natural Science Foundation of China (No.81803739).

Availability of data and materials The datasets generated during this work can be available on reasonable request.

Declarations

Ethics approval and consent to participate The processes involved in these biological experiments were approved by the Animal Research Ethics Committee of Tianjin University of Traditional Chinese Medicine (License No. TCM-LAEC2020075).

Consent for publication Manuscript is approved by all authors for publication.

Competing interests The authors declare no competing interests.

References

1. Li-Weber M. New therapeutic aspects of flavones: the anticancer properties of Scutellaria and its main active constituents Wogonin. Baicalein and Baicalin Cancer Treat Rev. 2009;35:57–68.
2. Liu Y, Wang B, Shu S, Li Z, Song C, Liu D, Niu Y, Liu J, Zhang J, Liu H, Hu Z, Huang B, Liu X, Liu W, Jiang L, Alami MM, Zhou Y, Ma Y, He X, Yang Y, Zhang T, Hu H, Barker MS, Chen S, Wang X, Nie J. Analysis of the Coptis chinensis genome reveals the diversification of protoberberine-type alkaloids. Nat Commun. 2021;12.
3. Xiao S, Liu C, Chen M, Zou J, Zhang Z, Cui X, Jiang S, Shang E, Qian D, Duan J. Scutellariae radix and coptidis rhizoma ameliorate glycolipid metabolism of type 2 diabetic rats by

modulating gut microbiota and its metabolites. Appl Microbiol Biot. 2020;104:303–17.
4. Schinella GR, Tournier HA, Prieto JM, Mordujovich DBP, Rios JL. Antioxidant activity of anti-inflammatory plant extracts. Life Sci. 2002;70:1023–33.
5. Wang S, Zheng Z, Weng Y, Yu Y, Zhang D, Fan W, Dai R, Hu Z. Angiogenesis and anti-angiogenesis activity of Chinese medicinal herbal extracts. Life Sci. 2004;74:2467–78.
6. Xiao S, Zhang Z, Chen M, Zou J, Jiang S, Qian D, Duan J. Xiexin Tang ameliorates dyslipidemia in high-fat diet-induced obese rats via elevating gut microbiota-derived short chain fatty acids production and adjusting energy metabolism. J Ethnopharmacol. 2019;241:112032.
7. Chen M, Wang P, Li T, Li L, Li J, Bai H, Lei H, Ma Q. Comprehensive analysis of Huanglian Jiedu decoction: Revealing the presence of a self-assembled phytochemical complex in its naturally-occurring precipitate. J Pharm Biomed Anal. 2021;195:113820.
8. Zhou X, Li H, Shi Z, Gao S, Wei S, Li K, Wang J, Li J, Wang R, Gong M, Zhao Y, Xiao X. Inhibition activity of a traditional Chinese herbal formula Huang-Lian-Jie-Du-Tang and its major components found in its plasma profile on neuraminidase-1. Sci Rep-Uk. 2017;7.
9. Liu Z, Wang W, Luo J, Zhang Y, Zhang Y, Gan Z, Shen X, Zhang Y, Meng X. Anti-apoptotic role of sanhuang xiexin decoction and anisodamine in endotoxemia. Front Pharmacol. 2021;12.
10. Xu X, Niu L, Liu Y, Pang M, Lu W, Xia C, Zhu Y, Yang B,Wang Q. Study on the mechanism of Gegen Qinlian Decoction for treating type II diabetes mellitus by integrating network pharmacology and pharmacological evaluation. J Ethnopharmacol. 2020;262.
11. Zhang C, Zhao R, Yan W, Wang H, Jia M, Zhu N, Zhu Y, Zhang Y, Wang P, Lei H. Compositions, formation mechanism, and neuroprotective effect of compound precipitation from the traditional Chinese prescription Huang-Lian-Jie-Du-Tang. Molecules. 2016;21:1094.
12. Jia D, Dou Y, Li Z, Zhou X, Gao Y, Chen K, Cong W, Ma M, Wu Z, Li W. Design, synthesis and evaluation of a baicalin and berberine hybrid compound as therapeutic agent for ulcerative colitis. Bioorgan Med Chem. 2020;28:115697.
13. Bernadett KK, Viktória J, Csilla TA, Balázs M, Pál TS, István A, Imre K, Péter K. Baicalin is a substrate of OATP2B1 and OATP1B3. Phytother Res. 2018;32.
14. Wang L, Kong H, Jin M, Li X, Stoika R, Lin H, Liu K. Synthesis of disaccharide modified berberine derivatives and their antidiabetic investigation in zebrafish using a fluorescence-based technology. Org Biomol Chem. 2020;18.
15. Chang D, Ma Y, Cao G, Wang J, Zhang X, Feng J, Wang W. Improved oral bioavailability for lutein by nanocrystal technology: Formulation development, in vitro and in vivo evaluation. Artificial cells, nanomedicine, and biotechnology. 2018;46:1018–24.
16. Brough C, Williams Iii RO. Amorphous solid dispersions and nano-crystal technologies for poorly water-soluble drug delivery. Int J Pharmaceut. 2013;453.
17. Miller JM, Beig A, Krieg BJ, Carr RA, Borchardt TB, Amidon GE, Amidon GL, Dahan A. The solubility–permeability interplay: Mechanistic modeling and predictive application of the impact of micellar solubilization on intestinal permeation. Mol Pharmaceut. 2011;8:1848–56.
18. Sahibzada MUK, Sadiq A, Zahoor M, Naz S, Shahid M, Qureshi NA. Enhancement of bioavailability and hepatoprotection by silibinin through conversion to nanoparticles prepared by liquid antisolvent method. Arab J Chem. 2020;13:3682–9.
19. Sahibzada MUK, Zahoor M, Sadiq A, Ur Rehman F, Al-Mohaimeed AM, Shahid M, Naz S, Ullah R. Bioavailability and hepatoprotection enhancement of berberine and its nanoparticles prepared by liquid antisolvent method. Saudi J Biol Sci. 2021;28:327–32.
20. Wang J, Tanaka T, Zhang H, Kouno I, Jiang Z. Formation and conformation of Baicalin-Berberine and Wogonoside-Berberine complexes. Chem Pharm Bull. 2012;60:706–12.
21. Yu F, He C, Waddad AY, Munyendo WLL, Lv H, Zhou J, Zhang Q. N-octyl-N-arginine-chitosan (OACS) micelles for gambogic acid oral delivery: Preparation, characterization and its study on in situ intestinal perfusion. Drug Dev Ind Pharm. 2013;40:774–82.
22. Pi J, Wang S, Li W, Kebebe D, Zhang Y, Zhang B, Qi D, Guo P, Li N, Liu Z. A nano-cocrystal strategy to improve the dissolution rate and oral bioavailability of baicalein. Asian J Pharm Sci. 2019;14.
23. Li W, Pi J, Zhang Y, Ma X, Zhang B, Wang S, Qi D, Li N, Guo P, Liu Z. A strategy to improve the oral availability of baicalein: The baicalein-theophylline cocrystal. Fitoterapia. 2018;129:85–93.
24. Li T, Wang P, Guo W, Huang X, Tian X, Wu G, Xu B, Li F, Yan C, Liang X, Lei H. Natural Berberine-Based Chinese herb medicine assembled nanostructures with modified antibacterial application. ACS Nano. 2019;13:6770–81.
25. Zhang X, Li Z, Gao J, Wang Z, Gao X, Liu N, Li M, Zhang H, Zheng A. Preparation of nanocrystals for insoluble drugs by Top-Down nanotechnology with improved solubility and bioavailability. Molecules. 2020;25:1080.
26. Li J, Jiang Q, Deng P, Chen Q, Yu M, Shang J, Li W. The formation of a host-guest inclusion complex system between beta-cyclodextrin and baicalin and its dissolution characteristics. J Pharm Pharmacol. 2017;69:663–74.
27. Xiao L, Poudel AJ, Huang L, Wang Y, Abdalla AM, Yang G. Nanocellulose hyperfine network achieves sustained release of berberine hydrochloride solubilized with β-cyclodextrin for potential anti-infection oral administration. Int J Biol Macromol. 2020;153.
28. Tinke AP, Vanhoutte K, De Maesschalck R, Verheyen S, De Winter H. A new approach in the prediction of the dissolution behavior of suspended particles by means of their particle size distribution. J Pharmaceut Biomed. 2005;39:900–7.
29. Muller RH, Jacobs C, Kayser O. Nanosuspensions as particulate drug formulations in therapy. Rationale for development and what we can expect for the future. Adv Drug Deliv Rev. 2001;47:3–19.
30. Sigfridsson K, Skantze U, Skantze P, Johansson S, Grant I, Smedsrød B, Fuglesteg B, Elvevold K, Lindfors L. Nanocrystal formulations of a poorly soluble drug. 1. In vitro characterization of stability, stabilizer adsorption and uptake in liver cells. Int J Pharmaceut. 2017;518:29–40.
31. Roos C, Dahlgren D, Sjögren E, Sjöblom M, Hedeland M, Lennernäs H. Jejunal absorption of aprepitant from nanosuspensions: Role of particle size, prandial state and mucus layer. Eur J Pharm Biopharm. 2018;132.
32. Daniela B, David P, Philipp S, Lisa E, Christine W, Christoph D, Alexander K, Hermann W, Charlotte K. Drug combinations and impact of experimental conditions on relative recovery in in vitro microdialysis investigations. Eur J Pharm Sci. 2019;127.